Spatially Resolved Atomic and Molecular Spectroscopy In Microelectronics Processing Plasmas

G. A. Hebner
Sandia National Laboratories
Albuquerque NM, 87185-1423

1. Introduction

Plasma processing of microelectronic materials is strongly dependent on the generation and control of neutral radial and ion species generated in a plasma. For example, process uniformity across a wafer is driven by a combination of plasma charged particle and neutral uniformity. Due to extensive research and engineering, the current generation of commercial plasma reactors can generate very radially uniform ion distributions, usually better than $\pm$ 2 percent as determined by ion saturation measurements. Due in part to the difficulty associated with determining the neutral radial distributions, control of the neutral radical uniformity is less well developed.

This abstract will review our recent measurements of the spatial distribution of several important atomic and molecular species in inductively coupled plasmas through Cl_2 / BCl_3 / Ar containing gas mixtures. Measured species include the ground state Cl and BCl densities as well as the metastable argon density. The focus of this review will be on the experimental techniques and results. In addition to assisting in the development of a fundamental understanding of the important plasma physics, these measurements have been used to benchmark multi dimensional plasma discharge codes.

Experimental setup

The experiments were performed in a Gaseous Electronics Conference (GEC) rf reference reactor that has been modified to include an inductively coupled plasma source (1). As shown in Fig. 1, the induction coil was a five turn, 11 cm diameter, planar coil constructed from 1/8 inch diameter copper tubing. The coil was separated from the plasma by a 1 cm thick fused silica window. Distance from the window to the lower electrode was 3.8 cm. For most of these experiments, the lower electrode was grounded, and covered with a 15 cm diameter, bare, unpatterned, silicon wafer. Due to the design of the reactor, the clear view between the ICP source and the lower electrode was approximately 13 cm in the radial direction and 3.1 cm in the axial direction. Both the induction coil and the lower electrode were water cooled.

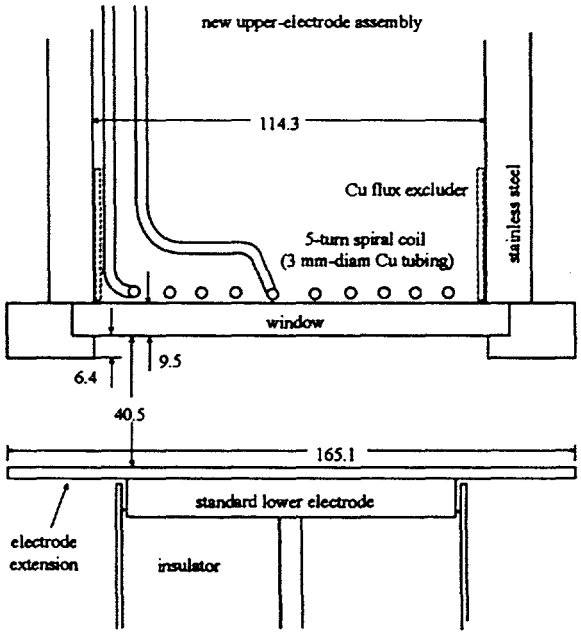

Figure 1 Cross section of the GEC rf reference cell showing the inductively coupled source

Operation frequency was 13.56 MHz. In this work, the reported rf power was the forward power minus the reflected power into the matching network. Previous work in this system has shown that for typical operating conditions, approximately 80 percent of the total input power was deposited into the plasma (2). For this experiment, the discharge chamber and associated hardware were mounted on a two dimensional translation table to facilitate spatial measurements without translating the optics.

DISCLAIMER

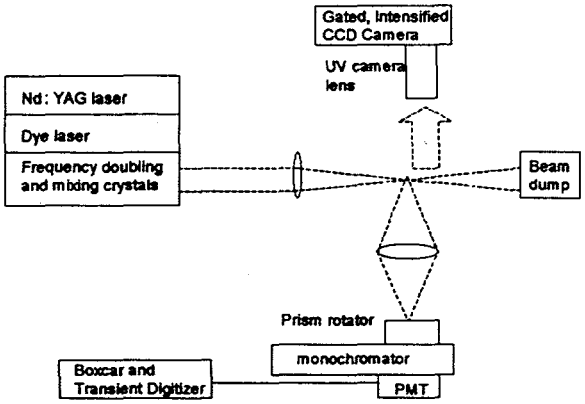

Figure 2 Typical experimental configureation. The LIF is detected using either a monochromator / PMT system or a gated CCD camera

A typical experimental configuration is shown in Fig. 2. A pulsed Nd:YAG pumped dye laser and associated frequency mixing and doubling crystals were used to generate the probe wavelengths. Typical pulse energies were 0.1 to 1 mJ, depending on the wavelength. Laser induced fluorescence (LIF) and plasma induced emission (PIE) were detected at right angles to the probe beam using either a monochromator / PMT configuration or a gated, intensified, bandpass filtered CCD camera. The CCD camera is equipped with a UV camera lens. For two photon LIF measurements of the atomic Cl density, a focusing lens was used to increase the laser power and improve the signal to noise ratio. However, for most single photon LIF experiments, the lens was not used. In the case of small LIF signals, a prism rotator was inserted before the monochromator to rotate the slits parallel to the laser probe.

Vignetting due to the discharge walls and windows was monitored by placing a 1 mm diameter point source (masked mercury spectral calibration lamp) in the center of the LIF observation area and translating the discharge chamber. For these measurements, vignetting was not a significant correction.

The choice of LIF detection scheme is influenced by the required information. Use of a monochromator / PMT system provides the relative species density and decay time at a given point in space. If collisional quenching due to neutral or electron collisions is spatially dependent, then a measurement of the decay lifetime is necessary to derive a relative density. For the case of our measurements of Cl and BCl density, the decay lifetime was less than 30 ns and did not vary with spatial position. However, the decay lifetime of the argon metastable was spatially dependent. While we have used the gated CCD to obtain some LIF images, the data discussed in the balance of this abstract was obtained using a PMT.

3. Spatially Resolved Measurements

3.1 BCl LIF and PIE

Relative BCl density was determined by LIF measurements in BCl_3 / Cl_2 / Ar gas mixtures (3). LIF was obtained by pumping ground state BCl at the Q-head in the (0,0) vibrational band of the $A^1\Pi$-$X^1\Sigma^+$ band system at 272 nm, and observing emission back to the ground state ($A^1\Pi$-$X^1\Sigma^+$) in the (0,1) vibrational band at 278 nm (4). Since the LIF was due to pumping from the ground state, which should be the most

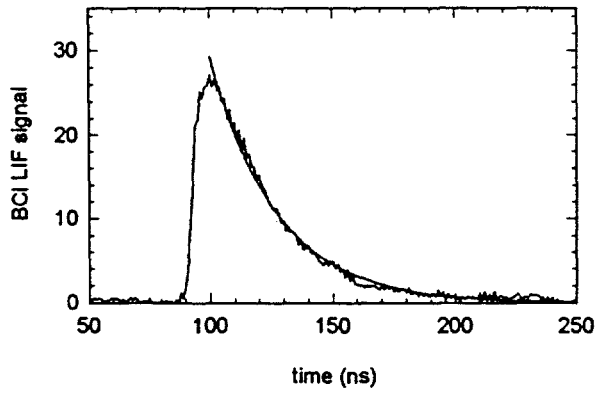

Figure 3 Typical LIF signal from BCl shown with a single exponential fit to the signal decay. The input power was 300 W at 20 mTorr in BCl_3. The fit decay time constant was 26 ns. LIF was obtained by pumping ground state BCl at the Q-head in the (0,0) vibrational band of the $A^1\Pi$-$X^1\Sigma^+$ band system at 272 nm, and observing emission back to the ground state ($A^1\Pi$-$X^1\Sigma^+$) in the (0,1) vibrational band at 278 nm.

heavily populated BCl state, this measurement yielded the relative BCl density in the discharge. A typical LIF signal obtained with this setup is shown in Fig. 3. Relative BCl density as reported here was obtained by fitting the decay curves, which were averaged over 256 shots, to a single exponential, and normalizing to the pump laser intensity. This procedure

compensated for possible changes in the quenching rate for the BCl excited state as the reactor parameters were changed, and also compensated for shot-to-shot variations in the laser energy. The uncertainty in the BCl density derived from the fits to the LIF decay is approximately +/- 7 percent of the maximum value for all the data presented. PIE emission from BCl was observed on the same transition (at 278 nm) as the LIF was observed. The LIF intensity is a measure of the ground state BCl density, and the PIE intensity is a measure of the excited state density: in general, these do not change in the same way as the reactor parameters are varied.

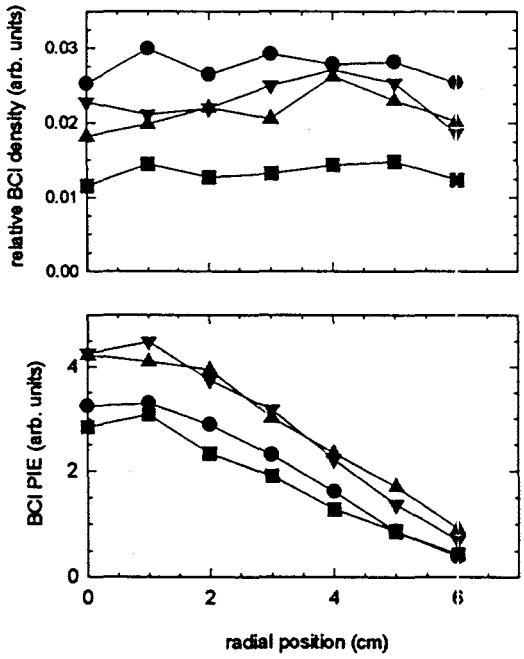

Figure 4 Relative BCl density and PIE as functions of radial position for various gas mixtures. Input power was 300 W at a reactor pressure of 20 mTorr. (●) indicates 10 sccm of BCl_3, (■) indicates 3.3 sccm of BCl_3 and 6.6 sccm of Ar, (▲) indicates 5 sccm of BCl_3 and 5 sccm of Cl_2, and (▼) indicates 8 sccm of BCl_3 and 2 sccm of N_2.

The uniformity of etch performance is partially determined by the distribution of neutral and ionic dissociation products in the plasma. Measurements of the BCl density and the PIE intensity as a function of radial position in the reactor are shown in Fig. 4. The BCl density was constant for all gas mixtures as a function of radial position, indicating that the BCl radical density was constant throughout the radial extent of the discharge; this measurement extended 1 cm beyond the edge of the rf coil. This implies that the BCl mean free path is large (approximately 3 to 5 cm) due to the low pressure in this plasma. The PIE intensity decreased with radial position, roughly tracking the electron density previously measured in these gas mixtures (5).

Axial variations in LIF and PIE intensity were also measured and are shown in Fig. 5. The LIF intensity decreased slightly from the lower electrode toward the upper electrode, indicating that the BCl density decreased slightly in this direction. The PIE intensity had the opposite trend, increasing slightly from the lower to the upper electrode. In Cl_2 and Ar/Cl_2 ICP discharges, the electron density, electron temperature, and the plasma potential increase from the lower to the upper electrode. Thus, the increase in PIE intensity shown in Fig. 5 is probably due to a similar axial increase in electron density and/or temperature in BCl_3 and BCl_3/Cl_2 mixtures.

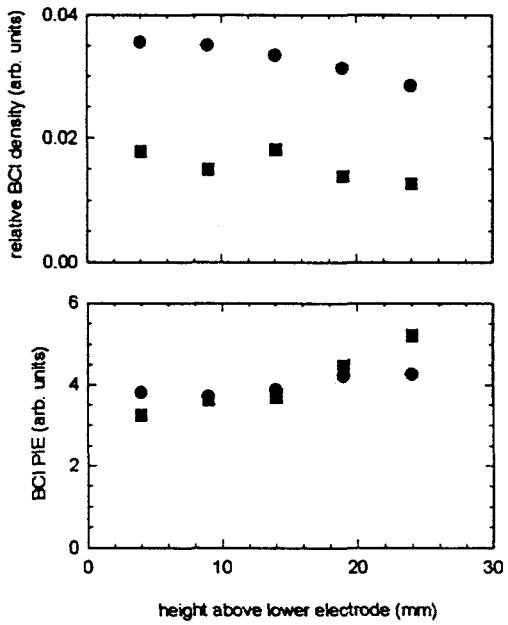

Figure 5 Relative BCl density and PIE as functions of axial position for various gas mixtures. Input power was 300 W at a reactor pressure of 20 mTorr. (●) indicates a pure BCl_3 discharge, and (■) indicates 3.3 sccm of BCl_3 and 6.6 sccm of Ar.

3.2 Cl LIF

For this work, two photons at 233.3 nm were used to excite the $3p^2P^0_{3/2}$ - $4p^4S^0_{3/2}$ transition (probing the lower level density of the spin split ground state). LIF on the $4p^4S^0_{3/2}$ - $4s^4P_{5/2}$ transition at 725.6 nm was recorded on a transient digitizer. For the range of conditions investigated in this work, collisional quenching of the upper state changed the measured LIF lifetime by less than ten percent (6).

While photodetachment of Cl^- to form Cl is undoubtedly present in this experiment, its impact on the relative atomic chlorine density measurements is believed to be minimal. Measurements suggest that the Cl_2 dissociation is greater than 70 percent for the operating conditions of this experiment (7,8). Thus, for the pressures used in this experiment, the atomic chlorine density is estimated to be on the order of 2×10^{14} cm^{-3}. Previous chlorine negative ion photodetachment measurements in this system have shown that the negative ion density is in the range of 5×10^{11} cm^{-3}, significantly below the estimated atomic chlorine density (9,10). Thus, the contribution of photodetached negative ions to the atomic chlorine signal is small for these plasma conditions.

Due to the high electric fields in the focus of the 233.3 nm pump beam, photodissociation of the Cl_2 or BCl_3 to form Cl could produce anomalous results. To investigate the influence of photodissociation on the observed signals, the Cl TALIF signal was first optimized at 20 mTorr with a discharge present. The discharge was then turned off and the cell filled with mixtures of Cl_2, BCl_3 or Ar to a static pressure of 10 Torr. For the case of pure Cl_2, no Cl signal was observed, even after significantly increasing the gain on the photomultipler tube. In the case of pure BCl_3 at 10 Torr, a signal of approximately one percent of the signal strength observed in the 20 mTorr discharge was observed. Dilution of the BCl_3 with Cl_2 or Ar resulted in a linear decrease in the Cl TALIF signal. Thus photodissociation of Cl_2 or BCl_3 did not contribute significantly to the Cl TALIF signal measured when the discharge was present.

The spatial distribution of atomic chlorine is shown in Fig. 6 as a function of radial position and Fig. 7 as a function of axial position. In all cases, the atomic chlorine density was constant with radial and axial position; this measurement extended 1 cm beyond the edge of the induction coil. Previous measurements of the BCl spatial distribution in this system showed the BCl spatial distribution was also constant as a function of radial position and increased slightly moving away from the

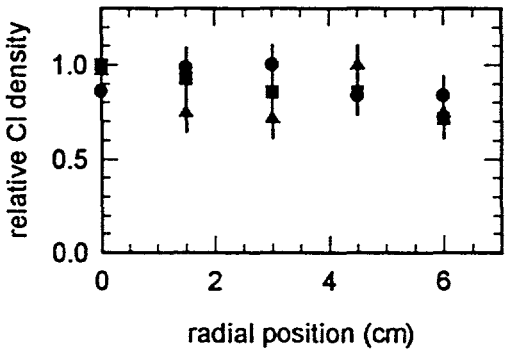

Figure 6 Relative chlorine density as a function of radial position. (●) denotes a Cl_2 discharge at 25 mTorr. (■) denotes a BCl_3 discharge at 20 mTorr. (▲) denotes a BCl_3 / Cl_2 discharge (3.3 / 6.6 sccm) at 20 mTorr. The input power was 300 W.

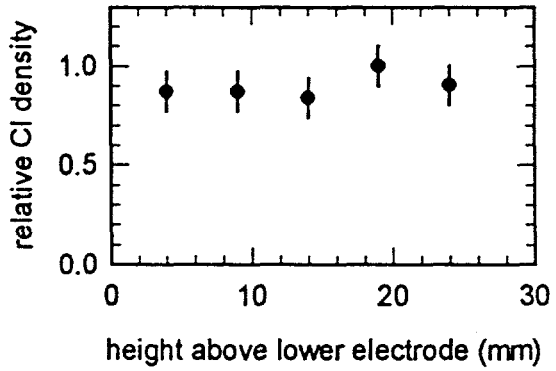

Figure 7 Relative chlorine density as a function of height above the lower electrode for a BCl_3 discharge. Power was 300 W at a pressure of 20 mTorr.

inductive coil. Spatially resolved negative ion measurements also showed the negative ion density was approximately flat with radial position (10). The constant neutral spatial distributions are in contrast with spatial distributions of the charged species. Langmuir

probe measurements of the spatial electron density and LIF measurements of the Cl^{+*} density showed the charged species were peaked in the center of the discharge with an approximate Gaussian profile with a FWHM of 8 cm (1,11).

3.3 Argon metastable LIF

The scaling of both the $1s_5$ and $1s_4$ argon excited states were investigated since the loss mechanisms are different for the two levels. The $1s_5$ level is metastable while the $1s_4$ level is radiatively allowed to the ground state but radiation trapped. For this work, a Nd:YAG pumped dye laser was frequency mixed to generate 395 and 404 nm radiation to excite the $1s_5$ to $3p_3$ and $1s_4$ to $3p_3$ transitions, respectively. The laser pulse width was approximately 8 ns and the energy was attenuated to 0.5 mJ per pulse. The laser was unfocused, with a beam diameter of approximately 6 mm. Fluorescence from the $3p_3$ to $1s_2$ transition at 433 nm was imaged onto the slits of a 0.46 m monochromator using a using a 150 mm focal length lens and a prism rotator to rotate the slit image parallel to the laser beam. The plasma observation volume was approximately 8 mm in the direction of the pump laser beam, 0.5 mm high and 4 mm wide. For each data point, fluorescence from 256 laser pulses was integrated using a transient digitizer. The LIF was observed to scale linearly with input energy. In all cases, the laser induced fluorescence was well fit by a single exponential decay. The relative density of the $1s_5$ and $1s_4$ levels was determined by the height of the exponential fit normalized to the laser power.

The relative density of the $1s_5$ and $1s_4$ levels in the center of the discharge as a function of rf power is shown in Fig. 8 for several pressures. These measurements were obtained 2 cm above the lower electrode and in the center of the discharge, r = 0 cm. The radial distribution for these conditions is shown in Fig. 9. As the power was increased, the $1s_5$ density in the center of the discharge decreased approximately 20 percent at 10 mTorr and 50 percent at 40 mTorr. The larger decrease with increased rf power for the 40 mTorr case was likely due to enhanced electron collisional mixing; the electron density increased at higher rf power and pressure (1). Looking at the radial profiles, as the power was increased, the $1s_5$ density in the center of the discharge decreased faster than the edges. This is consistent with an electron collisional process depopulating the density in the 1s5 level to the ground state in the center. Previous measurements of the spatial distribution of the electron density in this reactor geometry showed that the electron density peaked in the center of the plasma and had a Gaussian shape with a fwhm of 6 cm (1).

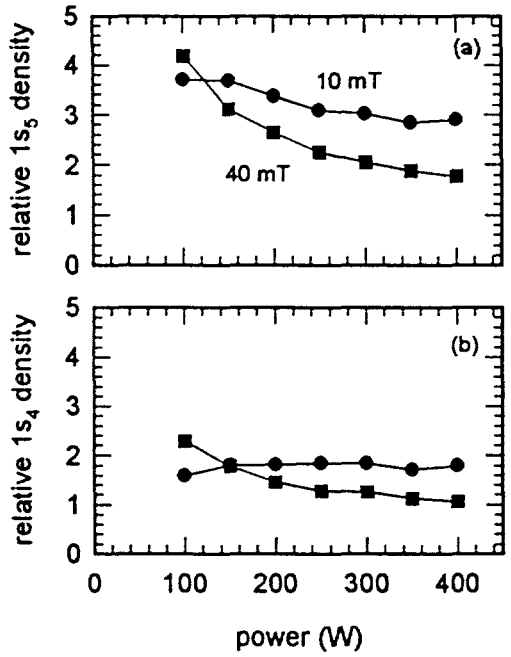

Figure 8 Relative $1s_5$ and $1s_4$ excited state densities in the center of the discharge as a function of power. Argon pressure was of 10 mTorr(●) and 40 mTorr(■), and height above the lower electrode was 2 cm.

The relative density of the $1s_4$ level has some similarities and notable differences with the power dependence of the $1s_5$ level. As the power was increased, the $1s_4$ density in the center of the 40 mTorr discharge also decreased approximately 50 percent. However, for the 10 mTorr case, the density of the $1s_4$ level increased slightly and then became constant. In addition to the density in the center increasing with rf power, the spatial distribution changed. As the rf power was increased, the $1s_4$ density in the center was approximately constant while the density at the edge decreased. The edge increase

may be due to enhanced electron collisional transfer from the $1s_5$ state at the

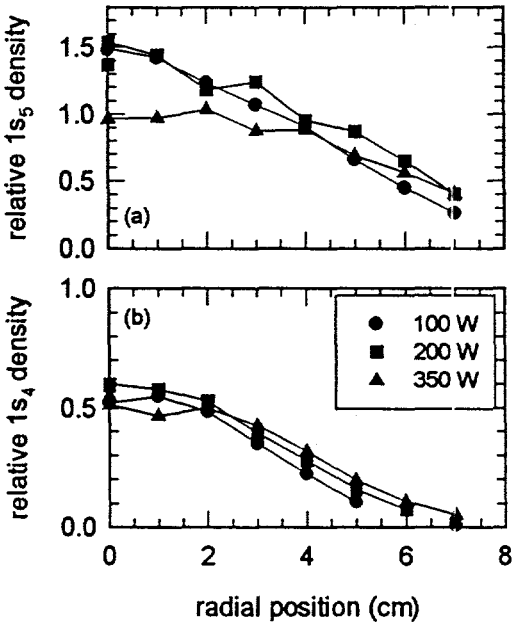

Figure 9 Relative $1s_5$ and $1s_4$ excited state densities as a function of radial position for powers of 100 W (●), 200 W (■) and 350 W (▲). The pressure was 10 mTorr and the height above the lower electrode was 2 cm.

edge as the power and electron density were increased. The differences in the $1s_4$ and $1s_5$ power dependence is likely due to the contributions of both radiation trapping and electron collisional transfer from the $1s_5$ state to the production / loss balance for the $1s_4$ level. As pressure and power increase, the importance of radiation trapping in enhancing the $1s_4$ density increases. In addition, increasing the electron density by increasing the pressure or power will increase the density of the $1s_4$ level due to enhanced collisional transfer from the $1s_5$ and $1s_3$ metastable levels.

The fluorescene lifetime was a function of power, pressure and radial position. Figure 10 shows the fluorescence lifetime as a function of radial position for several discharge conditions. The impact of electron collisional quenching were clearly observed in these measurements. In general, increasing the pressure decreased the LIF lifetime while the lifetime and quenching rate was a linear function of the rf power, as was the electron density (1).

The lifetimes were smallest for the highest powers and in the center of the discharge, where the electron density was maximum (1).

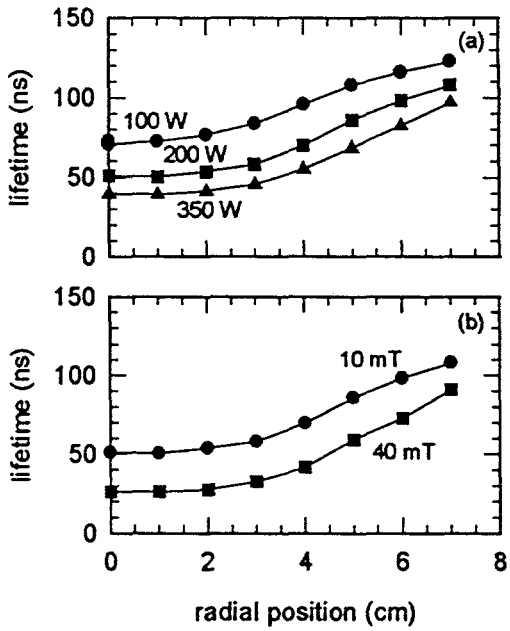

Figure 10 Fluorescence lifetime as a function of radial position. In figure (a) the pressure was 10 mTorr and in figure (b) the power was 200 W. Height above the lower electrode was 2 cm.

Measurements of fluorescence lifetime and quenching rates in the center of the discharge indicate the quenching rates were 2.8 x 10^{-8}, 5.6 x 10^{-8} and 8.8 x 10^{-8} cm^3 $atom^{-1}$ s^{-1} for rf powers of 100, 200 and 350 W respectively. In calculating the quenching rate, the pressure in the center of the discharge was reduced using the ideal gas law and the measured temperatures of 600, 800 and 1000 K for rf powers of 100, 200 and 350 W, respectively (2). The zero intercept gives lifetimes of 127, 104 and 67 nsec for rf power of 100, 200 and 350 W, respectively. Inoue et. al examined the radiative lifetime and collisional quenching rates for this transition in the afterglow of an argon discharge specifically to avoid the influence of electron collisions (12). For the $3p_3$ to $1s_2$ transition, they measured a lifetime of 123 ± 11 ns transition and a quenching rate constant of 4.2 x 10^{-10} cm^3 $atom^{-1}$ s^{-1}. At larger radial position, the lifetime increased, with a possible asymptote at approximately 130 - 140 ns, in line with the

measured lifetime of 123 ± 11 ns (12). Within our uncertainties, the quenching rates and lifetimes derived by extrapolating our measurements to zero power are consistent with the measurements of Inoue et al.

By combining these LIF measurements of the relative spatial metastable density and previous absolute line integrated density measurements along radial cords, information about the absolute spatially resolved density can be derived (2). In addition, it is possible to derive information about the spatial temperature distribution. In the previous analysis of the line integrated density, the absorption lineshape as a function of radial and axial position was recorded (2). The lineshapes were then fit to a theoretical Voigt lineshape that assumed a uniform temperature and density. While that assumption was clearly not correct in the light of these measurements, it was previously noted that a nonuniform spatial distribution would have the effect of averaging the density while not impacting the temperature due to the different influence of those two parameters on the integrated lineshape.

To simplify the derivation of an absolute density for the spatially resolved $1s_5$ level from the LIF and absorption measurements, we assumed a Gaussian functional form for the radial number density of

$$N_m(r) = N_0 \exp(-4\ln 2\,(r/\Delta dr_n)^2) \qquad (1)$$

where N_m is the radially dependent density, N_0 is the peak density and Δr_m is the FWHM of the distribution. An example of the fit for the spatially resolved $1s_5$ energy level in a 10 mTorr, 200 W discharge is shown in Fig. 11a. The measured LIF spatial profile was well fit by a Gaussian with a fwhm of 12 cm. The temperature profile is assumed to have a functional form of

$$T_m(r) = 300 + T_0 \exp(-4\ln 2\,(r/\Delta r_t)^2) \qquad (2)$$

where T_m is the radially dependent temperature, T_0 is the increase in the temperature above room temperature and Δr_t is the FWHM of the distribution. These radial density and temperature profiles were used to generate simulated absorption lineshapes along cords as a function of distance from the center of the discharge. The parameters of peak density, temperature and temperature FWHM where then optimized to give the best fit to the previously

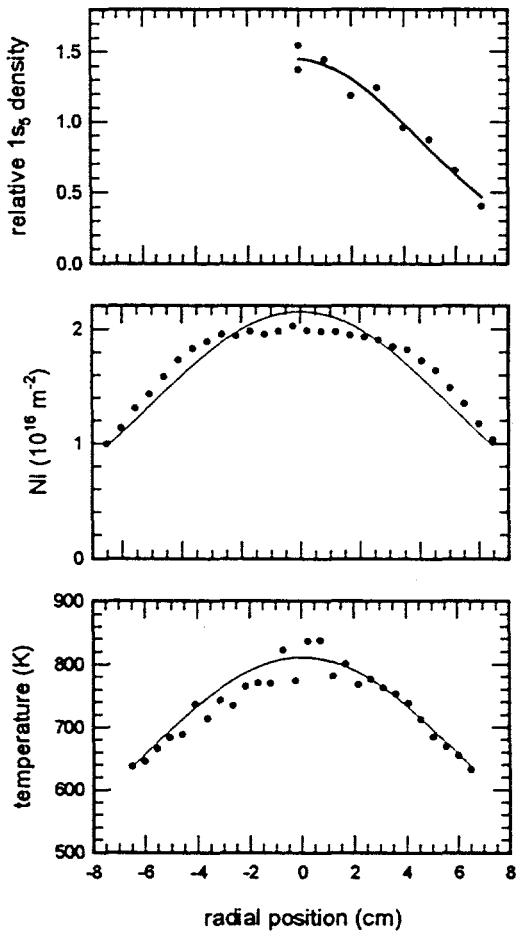

Figure 11 Relative $1s_5$ metastable density (a), line integrated density (b) and temperature (c) as a function of radial position for a power of 200 W and a pressure of 10 mTorr. The solid lines are fits to the data discussed in detail in the text.

measured line integrated density and temperature. The optimization routine was identical to the code used to fit the previous absorption data and used a downhill simplex method with simulated annealing to avoid local minima in the optimization. For the case shown in Fig. 11, the optimization routine returned a peak density of 3.4×10^{11} cm^{-3}, temperature of 300 + 550 = 850 K and a temperature FWHM of 16 cm. The resultant fits to the line integrated data capture most of the features of the previous

absorption data with the exception of the relatively constant line integrated density in the center of the discharge. This may due to the assumed Gaussian function for the density distribution. While a Gaussian profile appears to be correct in the center of the discharge, the values beyond r = 7 cm to the chamber windows may not be well fit by a Gaussian. An enhanced tail in the density distribution at r > 7 cm would result in the observed departure from the measured and fit line integrated density. The temperature of 850 K is in excellent agreement with the results of separate LIF measurements of the $1s_5$ temperature in the center of the discharge (2).

4.0 Acknowledgements

The Cl and BCl LIF measurements were performed with C. B. Fleddermann. The author thanks P. A. Miller, J. R. Woodworth, J. W. Alford, M. E. Riley and M. Blain for many helpful discussions. The technical assistance of T. W. Hamilton is gratefully recognized. This work was performed at Sandia National Laboratories and supported by the United States Department of Energy (DE-AC04-94AL85000). Sandia National Laboratories is operated by Sandia Corporation, a Lockheed Martin Company, for the U. S. Department of Energy.

5.0 References

1. P. A. Miller, G. A. Hebner, K. E. Greenberg, P. D. Pochan and B. P. Aragon, J. Resch. Natl. Int. Standard. Technol 100, 427 (1995).
2. G. A. Hebner, J. Appl. Phys. 80(6), 3215, 1996.
3. C. B. Fleddermann and G. A. Hebner, J. Appl. Phys. 83(8), 4030 (1998).
4. G. Herzberg and W. Hushley, Can. J. Res. 19A, 127 (1941).
5. G. A. Hebner, C. B. Fleddermann and P. A. Miller, J.Vac. Sci. Technol. A 15, 2698 (1997).
6. G. A. Hebner and C. B. Fleddermann, J. Appl. Phys. 83(10) 5102 (1998).
7. R. M. Forrister and H. M. Anderson, 48th Gaseous Electronics Conference, Berkeley CA, October 9 - 13, 1995, paper EA-8.
8. M. V. Malyshev and V. M. Donnelly, J. Vac. Sci. Technol. A 15, 550 (1997).
9. C. B. Fleddermann and G. A. Hebner, J. Vac. Sci. Technol. A, 15(4), 1955 (1997).
10. G. A. Hebner, J. Vac. Sci. Technol. A. 14(4), 2158 (1996).
11. G. A. Hebner, J. Appl. Phys. 80(6), 3215, 1996.
12. G. Inoue, D. W. Setser and N. Sadeghi, J. Chem. Phys., 76(2), 977 (1982).